

---

# Conformal retrofitting via Riemannian manifolds: distilling task-specific graphs into pretrained embeddings

---

Justin Dieter  
Stanford University  
jdieter@cs.stanford.edu

Arun Tejasvi Chaganty  
Square Inc.  
arun@squareup.com

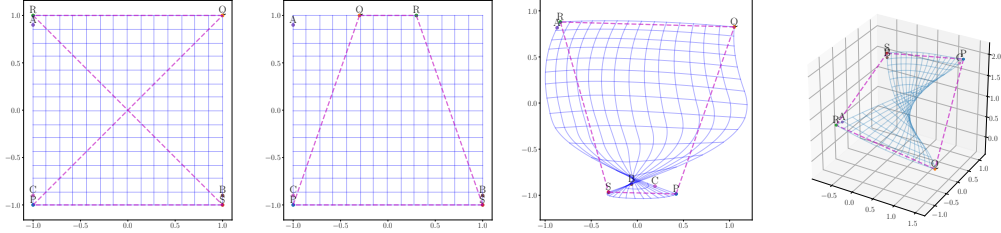
## Abstract

Pretrained (language) embeddings are versatile, task-agnostic feature representations of entities, like words, that are central to many machine learning applications. These representations can be enriched through *retrofitting*, a class of methods that incorporate task-specific domain knowledge encoded as a graph over a subset of these entities. However, existing retrofitting algorithms face two limitations: they overfit the observed graph by failing to represent relationships with missing entities; and they underfit the observed graph by only learning embeddings in Euclidean manifolds, which cannot faithfully represent even simple tree-structured or cyclic graphs. We address these problems with two key contributions: (i) we propose a novel regularizer, a *conformality regularizer*, that preserves local geometry from the pretrained embeddings—enabling generalization to missing entities and (ii) a new Riemannian feedforward layer that learns to map pre-trained embeddings onto a non-Euclidean manifold that can better represent the entire graph. Through experiments on WordNet, we demonstrate that the conformality regularizer prevents even existing (Euclidean-only) methods from overfitting on link prediction for missing entities, and—together with the Riemannian feedforward layer—learns non-Euclidean embeddings that outperform them.

## 1 Introduction

Pretrained embeddings [24, 29, 6, 31] and models [18, 13, 33, 34, 30, 5, 23] underpin many state-of-the-art results in computer vision and natural language processing across a variety of tasks and domains. These embeddings and models can be further improved for specific domains by using task-specific information, often encoded as a graph: word embeddings and language models better represent semantic similarity (as opposed to just distributional similarity) when combined with lexical ontologies [26]; image classifiers can generalize to new or rare classes when combined with knowledge graphs [36, 28, 3]; medical diagnoses can be improved when combined with medical knowledge graphs [21]; databases can impute missing data better when embeddings are specialized to their relational data [12].

Retrofitting methods incorporate these task-specific graphs either by directly translating the embeddings (standard retrofitting) [7, 26, 32, 10] or by learning a neural network to do the same (explicit retrofitting) [9, 16]. Both standard and explicit retrofitting represent new relationships between entities observed in the task-specific graph; however, it is important to consider their impact on *unobserved entities* because most task-specific graphs are characteristically incomplete (Figure 1). Standard retrofitting methods do not translate embeddings for unobserved entities and hence cannot capture relationships for these entities (Figure 1b). Explicit retrofitting methods do not preserve the geometry of pretrained embeddings and hence unintentionally modify relationships to and between unobserved entities (Figure 1c). We regard this as a problem of overfitting.



(a) Embeddings and graph (b) Standard Retrofitting (c) Explicit Retrofitting (d) Conformal Retrofitting

Figure 1: *Comparison of embeddings learned by various retrofitting methods.* Retrofitting methods transform pretrained embeddings to better represent a task-specific graph. Panel (a) illustrates an example of two-dimensional pretrained embeddings (ABC and PQRS), overlaid with the task-specific graph over entities PQRS; the entities ABC are missing from this graph. According to the graph, retrofitting methods should move P and Q closer to each other without also bringing P and R or Q and S together. (b) Standard retrofitting solves this problem by only moving the observed vertices, breaking the existing relationship between A and R, and failing to learn the one implied between A and B. (c) Explicit retrofitting learns a similar transformation using a continuous map that also applies to unobserved entities; now the relationship between A and R is preserved, but B and C have been forced together because the learned map does not preserve the geometry of the pretrained embeddings. (d) *Conformal retrofitting* introduces a *conformality* regularizer that explicitly preserves distances and angles; it results in a smoother transformation, resembling a saddle, which learns the relationship between A and B and preserves the (non-)relationship between B and C.

In this paper, we address the overfitting problem with a novel regularizer, a *conformality regularizer*, based on the pullback metric from Riemannian geometry. The regularizer directly encourages the learned transformation to preserve distances and angles around each embedding point, resulting in smoother transformations (Figure 1d). We also introduce a single hyper-parameter that allows for bounded distortions in distances while still preserving angles; our best results were obtained when moderate distortions are allowed.

The conformality regularizer naturally extends to non-Euclidean Riemannian manifolds; these manifolds have been shown to better represent graphs than the Euclidean manifolds used by existing retrofitting methods [27, 11, 1]. In fact, it is well-known that Euclidean manifolds require a logarithmic number of dimensions to represent even simple tree-structured graphs [14], while hyperbolic manifolds can represent such graphs with just two dimensions. We propose a new *Riemannian feedforward layer* that extends the conventional feedforward layer to arbitrary heterogeneous input and output manifolds. We use this new layer to transform pretrained embeddings from their Euclidean manifolds to a target Riemannian manifold.

We evaluate on predicting links to held out words from WordNet, a popular lexical knowledge graph used in a variety of language and vision tasks. On this task, we show that conformal regularization provides significant improvements to existing explicit retrofitting methods. Moreover, when combined with the proposed Riemannian feedforward layer, we find that non-Euclidean product manifolds such as  $\mathbb{S}^{30} \times \mathbb{H}^{30}$  improve link prediction scores not only for both held-out entities, but for entities observed during training time too.

In summary, our contributions are:

1. a novel regularization technique, conformality regularization, based on the pullback metric that better preserves angles and distances.
2. a new *Riemannian feedforward layer* that can operate on heterogeneous input and output manifolds.
3. experiments that show that conformal regularization improves the generalizability of existing explicit retrofitting methods and that product manifolds lead to better retrofitting.

## 2 Setup

Let us now setup notation and formally define retrofitting as a task. Our definitions expand prior work to apply when the pretrained and retrofitted embeddings lie on non-Euclidean Riemannian manifolds. We begin by reviewing some key concepts from Riemannian geometry.

### 2.1 Riemannian manifolds

A  $d$ -dimensional Riemannian manifold  $(M, g)$  is a smooth manifold  $M$  with an inner-product *metric*  $g$ ; for any point  $p \in M$ , there exists a tangent space  $T_p M$  that is isomorphic to  $d$ -dimensional Euclidean space  $\mathbb{R}^d$ . The metric  $g_p : T_p M \times T_p M \rightarrow \mathbb{R}$  smoothly varies with  $p \in M$ . Key examples of Riemannian manifolds include the Euclidean manifold  $\mathbb{E}$  with  $g_p^{\mathbb{E}}(x, y) = x^\top y$ ; the Poincare ball (an instance of a hyperbolic manifold)  $\mathbb{H}$  with  $g_p^{\mathbb{H}}(x, y) = \frac{2x^\top y}{1 - \|p\|^2}$ ; and the Spherical manifold with  $g_p^{\mathbb{S}}(x, y) = \frac{x^\top y}{\|x\|\|y\|}$ . Tangent spaces are regular vector spaces, allowing us to conveniently represent  $g_p$  as a matrix, also known as the metric tensor:  $G_p^{\mathbb{E}} = I$ ,  $G_p^{\mathbb{H}} = \frac{2}{1 - \|p\|^2} I$ .

The (geodesic) distance between two points on the manifold,  $d(x, y)$ , is defined to be the shortest path length between the two points:  $d(x, y) \stackrel{\text{def}}{=} \min_{\gamma} \int_0^1 \sqrt{g_{\gamma(t)}(\dot{\gamma}(t), \dot{\gamma}(t))} dt$ , where  $\gamma : [0, 1] \rightarrow M$  is any smooth curve starting at  $x$  and ending at  $y$ . We focus on Euclidean ( $\mathbb{E}$ ), spherical ( $\mathbb{S}$ ) and hyperbolic ( $\mathbb{H}$ ) manifolds and their products (defined below) which have efficient, closed-form solutions to the geodesic equation above.

Given two manifolds  $(M, g)$  and  $(N, g')$ , their product manifold  $M \times N$  has the following metric:  $\bar{g}_{(p,p')}((x, x'), (y, y')) = g_p(x, y) + g_{p'}(x', y')$ , where  $p \in M$ ,  $x, y \in T_p M$ ,  $p' \in N$  and  $x', y' \in T_{p'} N$ . Consequently, the geodesic on the product manifold also decomposes:  $\bar{d}((x, x'), (y, y'))^2 = d(x, y)^2 + d'(x', y')^2$ .

Finally, given  $p \in M$ , one can move to and from the tangent space using the log and exp maps: for  $q \in M$ , the logarithmic map  $\log_p(q)$  returns a vector  $v \in T_p M$  along the geodesic between the  $p$  and  $q$  of length  $d(p, q)$ ; for  $v \in T_p M$ , the exponential map  $\exp_p(v) \rightarrow q$  returns a point  $q \in M$  obtained by following the geodesic in the direction of  $v$  for a distance of  $\|v\|$ .  $\log_p$  and  $\exp_q$  are inverses of each other only when  $p = q$ ;  $\log_p(q)$  and  $\exp_p(v)$  is differentiable in  $p$ ,  $q$  and  $v$ .

### 2.2 Retrofitting

Let  $S$  be a pretrained source embedding in a given manifold  $(S, g^S)$  and  $\mathcal{G}(V, E)$  be the given (task-specific) graph, and  $T$  be the retrofitted target embeddings in a chosen target manifold  $(T, g^T)$ . We define  $V^S = \{v^S | v \in V\} \subset S$  to be the associated input embeddings of the vertices of the graph, and  $V^T = \{v^T | v \in V\} \subset T$  their corresponding target embeddings.

The goal of retrofitting is learn target embeddings  $T$  that: (a) faithfully represents distances in  $\mathcal{G}$  and (b) preserves the geometry of the source embeddings  $S$ . These two properties are typically captured by a multi-objective loss function using respective fidelity  $\ell_{\text{fid}}$  and preservation  $\ell_{\text{pre}}$  loss terms:

$$\mathcal{L} = \sum_{u, v \in E} \ell_{\text{fid}}(u, v) + \lambda \sum_{w \in V} \ell_{\text{pre}}(w), \quad (1)$$

where  $\lambda$  is a hyperparameter that balances the two objectives. Standard retrofitting [7] directly learns the target embeddings  $V^T$  with the following objective:

$$\mathcal{L}^{\text{SR}}(V^T) = \sum_{(u, v) \in E} \underbrace{\|u^T - v^T\|^2}_{\ell_{\text{fid}}^{\text{SR}}(u, v)} + \lambda \sum_{w \in V} \underbrace{\|w^T - w^S\|^2}_{\ell_{\text{pre}}^{\text{SR}}(w)}. \quad (2)$$

Explicit retrofitting [9] instead learns a neural network to transform the input embeddings,  $v^T = f_{\theta}(v^S)$ , with graph-distance based fidelity loss:

$$\mathcal{L}^{\text{ER}}(\theta) = \sum_{(u, v) \in E} \underbrace{\|d(u^T, v^T) - d_{\mathcal{G}}(u, v)\|^2}_{\ell_{\text{fid}}^{\text{ER}}(u, v)} + \lambda \sum_{w \in V} \underbrace{\|w^T - w^S\|^2}_{\ell_{\text{pre}}^{\text{ER}}(w)}, \quad (3)$$

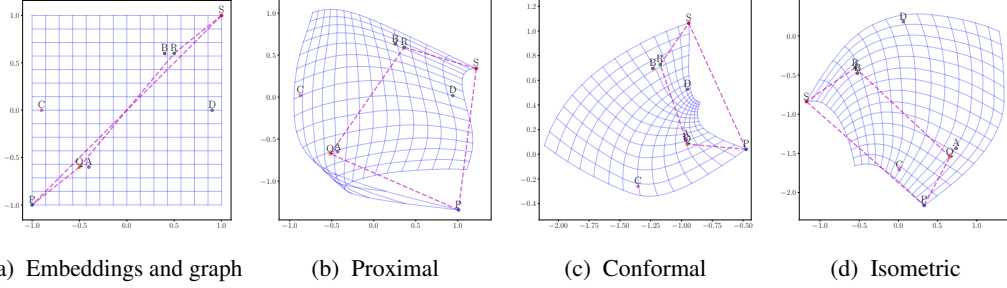


Figure 2: *Comparison of regularization methods for retrofitting.* (a) illustrates an example of given embeddings (ABCD and PQRS) and a cycle over the subset PQRS which are approximately collinear in the source embeddings; P and S start off far away from each other despite being neighbors in the graph. (b) The proximal regularizer used in prior work minimizes how far points in the image move without actually preserving spatial relationships from the input; in particular it learns a map that severely distorts the space between P and Q. (c-d) We propose a new *conformality regularizer* that allows points to move arbitrarily, but explicitly preserves spatial relationships such as angles (c) or distances (d) from the input; the learned maps transform space much more smoothly.

where  $d(u^\mathcal{T}, v^\mathcal{T})$  is one of Euclidean or cosine distance, and  $d_G(u, v)$  is the graph distance between the two vertices. Both methods share the same preservation loss, which we call *proximity regularization*:  $\ell_{\text{prox}}(w) = \|w^S - w^\mathcal{T}\|^2$ .

### 3 Conformal retrofitting

#### 3.1 Conformality regularization

Downstream methods rely on spatial relationships—distances and angles—between retrofitted embeddings. The proximity regularizer  $\ell_{\text{prox}}$  used by current retrofitting methods is often unable to preserve these relationships (Figure 2a). In this section, we propose a novel conformality regularizer that explicitly preserves local distances and angles in the image of the map  $f$ .

For any Riemannian manifold, the local geometry around a point  $p \in \mathcal{S}$  is defined by its tangent space  $T_p\mathcal{S}$ , and the Jacobian  $^1 \partial f_p : T_p\mathcal{S} \rightarrow T_{f(p)}\mathcal{T}$  describes how  $f$  transforms  $T_p\mathcal{S}$ . Using distances between points in this transformed tangent space,  $f$  induces a metric—the *pullback metric*  $\bar{f}$ —in the source manifold:  $\bar{f}_p(x, y) \stackrel{\text{def}}{=} g_{f(p)}^\mathcal{T}(\partial f_p(x), \partial f_p(y))$  for  $x, y \in \mathcal{S}$ . Written in more familiar matrix notation, the pullback metric tensor at  $p$  is:

$$F_p = J_p^\top G_{f(p)}^\mathcal{T} J_p, \quad (4)$$

where  $J_p$  is the Jacobian matrix at  $p$ , and  $G_{f(p)}^\mathcal{T}$  is the target metric tensor at  $f(p)$ .

When the pullback metric is equal to the original metric at  $p$ , so are distances and angles in its local geometry. This motivates an isometry regularizer that minimizes the difference between these metrics:

$$\ell_{\text{iso}}(p) = D(F_p, G_p^S), \quad (5)$$

where  $D$  is an appropriate distance function, and  $G_p^S$  is the source metric tensor. In practice, we use the geodesic distance on positive definite matrices  $D(X, Y) = \|\log(XY^{-1})\|^2$  [22], a symmetric loss function that is invariant to scalar transformations, congruence transformations and inversion. For example, if both the target metric and the original metric are the identity and representative of Euclidean space, this objective will encourage the Jacobian to be unitary at all points. We note that the  $G_p^S$  and  $G_{f(p)}^\mathcal{T}$  are defined by the given manifolds, and  $J_p$  can be easily computed using automatic differentiation.

The isometry regularizer already improves on the proximity regularizer in encouraging smoother maps in Figure 2d; most notably, it generally preserves the areas of each grid square in the image.

<sup>1</sup>In differential geometry,  $\partial f_p$  is better known as the *pushforward* or differential.

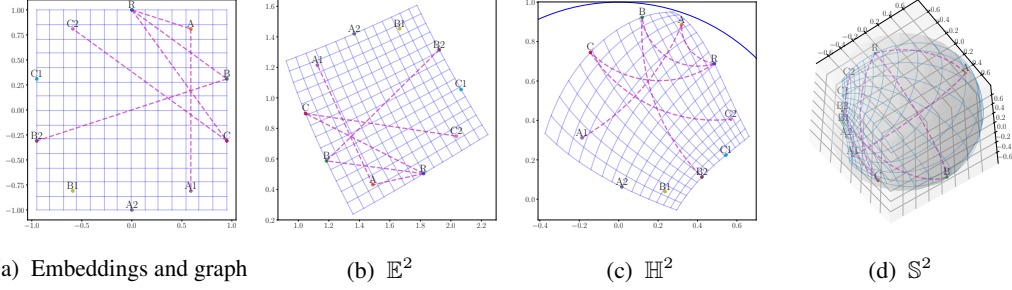


Figure 3: Comparison of target manifolds when retrofitting given pretrained embeddings (R, A, B, C, A1, A2, B1, B2, C1 and C2) to a tree over the subset R, A, B, C, A1, B1, C2 (a). The Euclidean manifold is unable to properly represent the graph without severely distorting space (b). The Hyperbolic manifold perfectly represents the graph by exploiting its unique geometry; it embeds points near the edge of the Poincaré ball (drawn in blue) where space is sufficiently stretched to ensure that the distance between B and B2 is actually far less than the distance between (say) B and C (c). The Spherical manifold perfectly represents the graph by exploiting its geometry; A is able to be close to A1, A2 (similarly for B and C) by following a path on the far side of the sphere (d).

When angular information is more important than distances, we can relax the equality constraint to one that bounds the ratio between the two metrics:

$$\ell(p) = D(F_p, e^\alpha G_p^S) \quad \text{subj. to } -C \leq \alpha \leq C,$$

where  $\alpha$  is a free parameter and  $C$  is the desired bound. In the supplementary material, we solve for KKT conditions and show that when  $D$  is the geodesic distance, the above constrained objective reduces to the following unconstrained objective:

$$\ell_{\text{conf}}(p) = \left\| \log \left( F_p G_p^{S^{-1}} \right) \right\|^2 - \min \left\{ C, \log \det \left( F_p G_p^{S^{-1}} \right)^2 \right\}. \quad (6)$$

We call  $\ell_{\text{conf}}$  the conformality regularizer; when  $C = 0$  it reduces to (5) and preserves distances; when  $C \rightarrow \infty$  it only preserves angles (Figure 2c). Like the geodesic distance, it is invariant to scalar and congruence transformations, as well as matrix inversion.

In the supplementary material, we prove that optimizing this regularizer over the input space is both necessary and sufficient for  $f$  to be an isometric and/or conformal map:

**Theorem 1.** *For all values of  $C$ ,  $f$  is a conformal map iff  $\ell_{\text{conf}}(w) = 0$  for all points  $w \in \mathcal{S}$ ; if  $C = 0$ , then  $f$  is a isometric map iff  $\ell_{\text{conf}}(w) = 0$  for all points  $w \in \mathcal{S}$ .*

### 3.2 Riemannian feed forward layers

So far, our focus has been on learning Euclidean target embeddings. However, for many graphs Euclidean manifolds can require far more dimensions than non-Euclidean manifolds [14, 27, 11]; this problem is only exacerbated if spatial relationships from the input must be maintained. Figure 3 provides one such example where non-Euclidean manifolds, unlike the Euclidean one, are able to exploit their unique geometry to fit a graph while maintaining spatial relationships. We generalize standard feedforward layers to accept and project embeddings on general Riemannian manifolds.

A typical (Euclidean) feedforward layer (EFL) transforms input  $x \in \mathbb{R}^m$  by applying a linear transform  $A \in \mathbb{R}^{n \times m}$ , followed by a translation by  $b \in \mathbb{R}^n$  and a pointwise nonlinearity  $\sigma$ :  $\text{EFL}(x) \stackrel{\text{def}}{=} \sigma(Ax + b)$ . However, none of these steps have direct analogs in Riemannian geometry. We overcome this limitation by applying the transforms in Euclidean tangent spaces using the log and exp maps; the Riemannian feedforward layer (RFL) from source manifold  $\mathcal{S}$  and target manifold  $\mathcal{T}$  is:

$$\text{RFL}(x^{\mathcal{S}}) \stackrel{\text{def}}{=} \exp_{b^{\mathcal{T}}} \left( \sigma \left( A \log_{b^{\mathcal{S}}} x^{\mathcal{S}} \right) \right), \quad (7)$$

where  $b^{\mathcal{S}} \in \mathcal{S}$ ,  $b^{\mathcal{T}} \in \mathcal{T}$  are distinct bias terms and  $A : T_{b^{\mathcal{S}}} \mathcal{S} \rightarrow T_{b^{\mathcal{T}}} \mathcal{T}$  is a linear operator between the source and target tangent spaces. For the manifolds considered in this paper, which are *geodesically*

complete, we can represent  $A$  as a matrix in  $\mathbb{R}^{n \times m}$ , where  $m$  and  $n$  are respectively the dimensions of the source and target manifolds. When applied to Euclidean manifolds, RFL reduces to EFL when  $b^T = 0$  and  $b^S = -A^\dagger b$ ; while the two bias terms are redundant in this case, they are necessary for Riemannian manifolds that do not contain a  $0$  element like  $\mathbb{S}$ . Derivatives for all of these parameters can be efficiently computed through automatic differentiation.

Like typical feedforward layers, two Riemannian feedforward layer can be stacked when the output manifold of the first layer is the input manifold of the second. We call such stacked Riemannian feedforward layers *Riemannian feedforward networks*.

### 3.3 Putting it together: conformal retrofitting

The final component of a retrofitting method is the fidelity loss  $\ell_{\text{fid}}$  used to encourage graph neighbors to be closer to each other in the target embeddings. We found that a manifold-aware max-margin loss worked best:

$$\ell_{\text{fid}}^{\text{CR}}(u, v) = \sum_{x^T \in \mathcal{N}(u^T)} \max(0, \gamma + d(u^T, v^T) - d(u^T, x^T)), \quad (8)$$

where  $\gamma$  is the margin,  $\mathcal{N}(u^T)$  is the set of neighbors to  $u^T$  in the target manifold excluding any graph neighbors; the distances,  $d(u^T, v^T)$  and  $d(u^T, x^T)$ , are also measured in the target manifold.

Putting all these pieces together, we propose a new retrofitting method, *conformal retrofitting*, that transforms pretrained embeddings using a Riemannian feedforward network,  $u^T = f_\theta(u^S)$  and is trained with the following objective:

$$\mathcal{L}^{\text{CR}} = \sum_{(u, v) \in E} \ell_{\text{fid}}^{\text{CR}}(u, v) + \lambda \sum_{w \in V} \underbrace{\ell_{\text{conf}}(w^S)}_{\ell_{\text{pre}}^{\text{CR}}(w)}. \quad (9)$$

## 4 Experiments

### 4.1 Training details

We use Riemannian Stochastic Gradient Descent (R-SGD) [2]—an extension of stochastic gradient descent that efficiently projects gradient updates from the tangent space onto the manifold—to train parameters of non-Euclidean Riemannian feedforward layers, and Adam [17] to train the remaining Euclidean parameters. We found that the relative scales of the fidelity and preservation losses changed significantly over the course of training and a static objective weight  $\lambda$  would only train one of the two losses. To solve this problem, we used GradNorm [4], an adaptive loss balancing algorithm that weighs objectives inversely proportional to norm of their gradients; we found it necessary to modify the algorithm to use the geometric mean of gradient norms instead of the arithmetic mean to be more robust to outliers.

The max-margin loss  $\ell_{\text{fid}}^{\text{CR}}$  uses nearest neighbors in  $V^T$ . During training, we sampled 50 manifold neighbors for each point in a mini-batch. While a number of fast exact and approximate near neighbor algorithms exist for Euclidean embeddings, they rely on fast distance and mean computations. Both of these operations can be significantly slower for non-Euclidean manifolds, even those with closed-form distance functions like  $\mathbb{H}$  or  $\mathbb{S}$ . Following Turaga and Chellapa [35], we overcome this bottleneck by projecting  $V^T$  onto the tangent space at their centroid:  $\arg \min_{c \in \mathcal{T}} \sum_{v^T \in V^T} d(c, v^T)^2$ . We then build an efficient nearest neighbor index over these Euclidean projections using the FAISS library [15]; the index is periodically updated as the model trains.

### 4.2 Evaluation setup

For all experiments below, we used 50-dimensional pretrained GloVe embeddings [29] as our source embeddings, two Euclidean intermediate layers in  $\mathbb{E}^{1600}$  and vary the target manifold.<sup>2</sup> We restricted intermediate layers for all methods to be Euclidean to fairly compare with explicit retrofitting, and to focus our hyper-parameter search on the target manifold. When picking the search space for the target manifold, we focused on two settings: (a) where the total dimensions were equal to the source

<sup>2</sup>The dimensionality of the intermediate layers were chosen after an initial random grid search.

Retrofitting Method		Train mAP	Test mAP	Retrofitting Method		Train mAP	Test mAP
Original ( $\mathbb{S}^{50}$ )		9.9%	7.9%	Original ( $\mathbb{S}^{50}$ )		25.1%	21.5%
Explicit ( $\mathbb{S}^{50}$ )		11.5%	8.9%	Explicit ( $\mathbb{S}^{50}$ )		<b>73.4%</b>	<b>26.3%</b>
Conformal	$-\log(C)$			Conformal	$-\log(C)$		
$\mathbb{S}^{50}$	1.0	11.6%	9.0%	$\mathbb{S}^{50} \times \mathbb{E}^5 \times \mathbb{H}^5$	0.6	69.4%	25.6%
$\mathbb{S}^{30} \times \mathbb{E}^{30}$	0.2	11.9%	9.2%	$\mathbb{S}^{30} \times \mathbb{E}^{30}$	0.4	45.2%	26.0%
$\mathbb{S}^{60}$	0.8	11.9%	<b>9.3%</b>	$\mathbb{S}^{45} \times \mathbb{E}^5$	0.6	34.9%	26.1%
$\mathbb{S}^{30} \times \mathbb{H}^{30}$	0.2	<b>12.8%</b>	<b>9.3%</b>	$\mathbb{S}^{50} \times \mathbb{E}^{10}$	0.2	52.9%	<b>26.3%</b>

(a) NOUNS
(b) MAMMALS

Table 1: *Link prediction scores measured using mean average precision (mAP) on two hypernymy datasets (NOUNS and MAMMALS). We report conformality as  $-\log(C)$ , with a value of 0 corresponding to  $C = \infty$ , to better represent its range. On NOUNS, conformal retrofitting improves test mAP scores over explicit retrofitting even in the original  $\mathbb{S}^{50}$  manifold; the best results are obtained in higher dimensions. On both datasets, mixed non-Euclidean manifolds significantly improve train mAP scores, reflecting their better ability to represent the graph seen during training.*

embeddings (50-dimensional) to compare with baselines, and (b) where they were slightly larger (60-dimensional) to explore the benefits of added dimensions. In each setting, we explored both pure manifolds (e.g.  $\mathbb{S}^{50}$ ) and product manifolds that either were a balanced or skewed split.

Additionally, for each target manifold, we tuned conformality and learning rate using random grid search. The conformality parameter ( $-\log(C)$ ) was chosen using uniformly spaced values from its entire range: 0, 0.2, 0.4, 0.6, 0.8, 1. Finally, we ran each hyperparameter combination once and report the results of the best model (using validation metrics) in each hyperparameter sweep. In our final experiments, we selected the baseline model (explicit retrofitting) from a sweep of 30 runs for each dataset, and the proposed conformal retrofitting model from a sweep (that included the target manifold and conformality as hyperparameters) of 60 runs for each dataset. All results are presented using early stopping on the validation set.

We evaluate the above retrofitting methods using two datasets constructed from the WordNet [25] graph: the hierarchy of all 1,180 mammals connected via a hypernymy relation (MAMMALS), and the hierarchy of all 82,061 nouns connected via a hypernymy relation (NOUNS). The nodes of datasets were split into train, validation and test sets using a 80 :: 10 :: 10 split. While the train set only contains edges between its nodes, the validation set includes edges to the train set and the test set includes edges to both train and validation sets.

Similar to Glavaš and Vulić [9], we measure similarity using cosine distance, which is equivalent to being embedded on  $\mathbb{S}$ . Glavaš and Vulić [9] use a slightly different contrastive loss and method to sample near neighbors. To fairly compare our methods, we reimplement explicit retrofitting using our max margin loss and neighborhood sampling with the proximal regularizer. We use mean average precision (mAP) to evaluate each methods ability to predict hypernymy relations (edges) to words (nodes) not seen during training. We also report scores on metrics achieved by the original GloVe embeddings.

Additional details, dataset statistics and a complete list of chosen hyperparameters are provided in the supplementary material.

### 4.3 Results

On NOUNS, conformal retrofitting significantly improves test mAP scores when targeting higher dimensional manifolds Table 1, while still providing improvements in source manifold  $\mathbb{S}^{50}$ . While purely spherical manifolds ( $\mathbb{S}^{60}$ ) have similar test link prediction scores as mixed manifolds ( $\mathbb{S}^{30} \times \mathbb{H}^{30}$ ) the latter is significantly better at representing the train graph. On MAMMALS, conformal retrofitting does not provide significant improvements over explicit retrofitting; this is likely due to the small size of the dataset. However, because MAMMALS is a more structured graph, we found that mixed manifolds did significant better than their pure counter parts, both on train and test mAP scores.

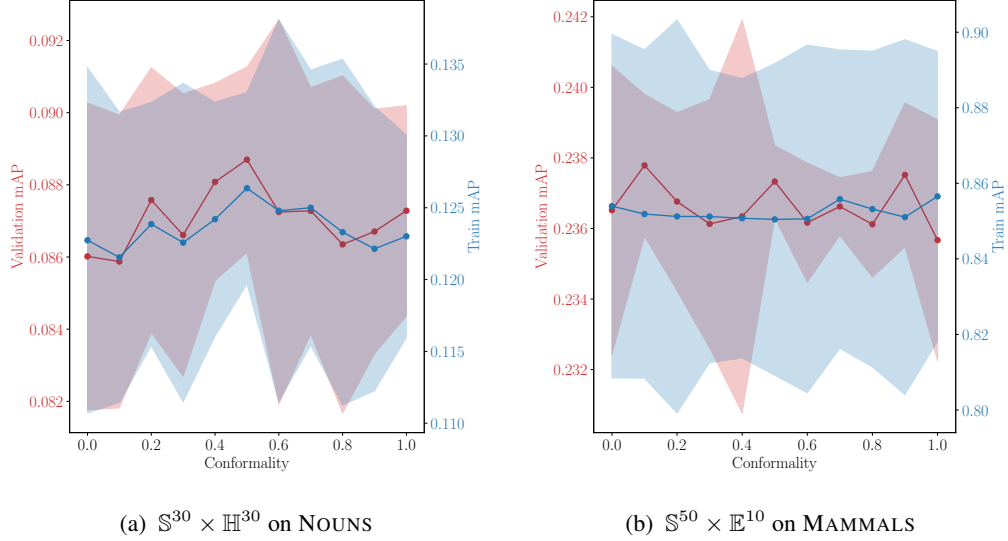


Figure 4: *Impact of conformality on train and validation mAP scores for top-performing target manifolds.* Each point is the average over 5 runs; the shaded region highlights a single standard deviation. We report conformality as  $-\log(C)$ , with a value of 0 corresponding to  $C = \infty$ , to better represent its range. For  $\mathbb{S}^{30} \times \mathbb{H}^{30}$  on NOUNS, we find that an intermediate values perform best on both train and validation mean average precision (mAP); for  $\mathbb{S}^{50} \times \mathbb{E}^{10}$  on MAMMALS, conformality plays less of a role. In the appendix, we show that conformality plays a significant role for other target manifolds on MAMMALS.

The conformality hyper-parameter values lie in-between the two extremes, indicating that while slight distortions to distances helps the model fit the graph better, they remain important (Figure 4).

## 5 Related Work

There are several alternatives to retrofitting when combining task-specific graphs with distributional data: Wang et al. [36], Peng et al. [28], Chen et al. [3] encode the task-specific graph as a graph convolutional network that transforms pretrained word embeddings into (visual) object classifiers for unknown or rare labels; Kumar and Araki [19] incorporate relational constraints from the graph as an additional subspace constraint when learning word-vectors; Lauscher et al. [20] introduce a new pre-training task to predict relations from the graph for contextual embedding models like BERT [5].

The topic of better representing graph structures has been well studied: Mrkšić et al. [26], Glavaš and Vulić [10], Rothe and Schütze [32] extend similarity-based retrofitting [7] to include antonymy and directional lexical entailment relations through relation-specific loss objectives complimentary to our own; Nickel and Kiela [27] show that hyperbolic manifolds could better represent tree-structured graphs, while Gu et al. [11] show that the mixed product-manifolds studied in this paper can better represent more complex graphs in low dimensions; Balažević et al. [1] apply hyperbolic manifolds to multi-relational graphs.

Riemannian feed-forward layers extend hyperbolic neural networks [8], which are explicitly parameterized for hyperbolic manifolds, to arbitrary Riemannian manifolds. To the best of our knowledge, ours is the first work to define fully-differentiable layers between arbitrary Riemannian manifolds.

## 6 Conclusions

In this paper, we introduce a new retrofitting method, conformal retrofitting, that can successfully combine task-agnostic representations with graph-structured, task-specific information to produce powerful pretrained embeddings that can be effectively utilized by downstream tasks in natural language and vision. Specifically, our method comprises of two novel components that we develop:



(i) a conformality regularizer using the pullback metric from Riemannian geometry, which explicitly encourages the map to preserve angles and distances; and (ii) a new neural network layer (the Riemannian feedforward layer) that can learn mappings to non-Euclidean manifolds (to faithfully represent graph structure). This enables conformal retrofitting to address key limitations of existing retrofitting algorithms. We demonstrate the efficacy of conformal retrofitting through experiments on synthetic data with known ground truth structure and on WordNet where conformal retrofitting outperforms existing algorithms by learning embeddings in non-Euclidean product manifolds. Our contributions provide an important foundation for future work on both task-specific embeddings, and performance improvements on new downstream applications.

## Broader Impact

This work is primarily focused on introducing fundamental algorithms and core analysis for pretrained embeddings. We believe better such algorithms may be helpful for reducing the compute, energy and carbon footprints of developing ML models due to more effective representations and feature reuse. However, all such algorithms must be trained on well curated, and representative datasets, and should be thoroughly validated to detect potential biases.

## References

- [1] I. Balažević, C. Allen, and T. Hospedales. Multi-relational poincaré graph embeddings. *arXiv preprint arXiv:1905.09791*, 2019 2019 2019.
- [2] S. Bonnabel. Stochastic gradient descent on riemannian manifolds. *IEEE Transactions on Automatic Control*, 58(9):2217–2229, 2013.
- [3] R. Chen, T. Chen, X. Hui, H. Wu, G. Li, and L. Lin. Knowledge graph transfer network for few-shot recognition. *arXiv preprint arXiv:1911.09579*, 2019.
- [4] Z. Chen, V. Badrinarayanan, C. Y. Lee, and A. Rabinovich. GradNorm: Gradient normalization for adaptive loss balancing in deep multitask networks. *35th International Conference on Machine Learning, ICML 2018*, 2:1240–1251, 2018.
- [5] J. Devlin, M. Chang, K. Lee, and K. Toutanova. BERT: Pre-training of deep bidirectional transformers for language understanding. In *Association for Computational Linguistics (ACL)*, pages 4171–4186, 2019.
- [6] J. Donahue, Y. Jia, O. Vinyals, J. Hoffman, N. Zhang, E. Tzeng, and T. Darrell. Decaf: A deep convolutional activation feature for generic visual recognition. In *International Conference on Machine Learning (ICML)*, volume 32, pages 647–655, 2014.
- [7] M. Faruqui, J. Dodge, S. K. Jauhar, C. Dyer, E. Hovy, and N. A. Smith. Retrofitting word vectors to semantic lexicons. In *Human Language Technology and North American Association for Computational Linguistics (HLT/NAACL)*, pages 1606–1615, 2015.
- [8] O. Ganea, G. Bécigneul, and T. Hofmann. Hyperbolic neural networks. *arXiv preprint arXiv:1805.09112*, 2018.
- [9] G. Glavaš and I. Vulić. Explicit retrofitting of distributional word vectors. In *Association for Computational Linguistics (ACL)*, pages 34–45, 2018.
- [10] G. Glavaš and I. Vulić. Monolingual and cross-lingual lexical entailment. In *Association for Computational Linguistics (ACL)*, pages 4824–4830, 2019.
- [11] A. Gu, F. Sala, B. Gunel, and C. Ré. Learning mixed-curvature representations in products of model spaces. In *International Conference on Learning Representations (ICLR)*, 2019.
- [12] M. Günther, M. Thiele, and W. Lehner. Retro: Relation retrofitting for in-database machine learning on textual data. *arXiv preprint arXiv:1911.12674*, 2019.
- [13] K. He, X. Zhang, S. Ren, and J. Sun. Deep residual learning for image recognition. *2016 IEEE Conference on Computer Vision and Pattern Recognition (CVPR)*, pages 770–778, 2016.
- [14] M. Jiří. On embedding trees into uniformly convex banach spaces. *Israel Journal of Mathematics*, 114:221–237, 1999.
- [15] J. Johnson, M. Douze, and H. Jégou. Billion-scale similarity search with gpus. *arXiv preprint arXiv:1702.08734*, 2017.

- [16] A. Kamath, J. Pfeiffer, E. M. Ponti, G. Glavaš, and I. Vulić. Specializing distributional vectors of all words for lexical entailment. In *Workshop on Representation Learning for NLP*, pages 72–83, 2019.
- [17] D. Kingma and J. Ba. Adam: A method for stochastic optimization. *arXiv preprint arXiv:1412.6980*, 2014.
- [18] A. Krizhevsky, I. Sutskever, and G. E. Hinton. Imagenet classification with deep convolutional neural networks. In *Advances in Neural Information Processing Systems (NeurIPS)*, pages 1097–1105, 2012.
- [19] A. Kumar and J. Araki. Incorporating relational knowledge into word representations using subspace regularization. *54th Annual Meeting of the Association for Computational Linguistics, ACL 2016 - Short Papers*, pages 506–511, 2016.
- [20] A. Lauscher, I. Vulić, E. M. Ponti, A. Korhonen, and G. Glavaš. Informing unsupervised pretraining with external linguistic knowledge. *arXiv preprint arXiv:1909.02339*, 2019.
- [21] X. Li, Y. Wang, D. Wang, W. Yuan, D. Peng, and Q. Mei. Improving rare disease classification using imperfect knowledge graph. *BMC Medical Informatics and Decision Making*, 19(5):238, 2019.
- [22] L.-H. Lim, R. Sepulchre, and K. Ye. Geometric Distance Between Positive Definite Matrices of Different Dimensions. *IEEE Transactions on Information Theory*, 65(9):5401–5405, 2019.
- [23] Y. Liu, M. Ott, N. Goyal, J. Du, M. Joshi, D. Chen, O. Levy, M. Lewis, L. Zettlemoyer, and V. Stoyanov. Roberta: A robustly optimized bert pretraining approach. *arXiv preprint arXiv:1907.11692*, 2019.
- [24] T. Mikolov, I. Sutskever, K. Chen, G. S. Corrado, and J. Dean. Distributed representations of words and phrases and their compositionality. In *Advances in Neural Information Processing Systems (NeurIPS)*, pages 3111–3119, 2013.
- [25] G. A. Miller. WordNet: a lexical database for english. *Journal of the ACM (JACM)*, 38:39–41, 1995.
- [26] N. Mrkšić, I. Vulić, D. Ó. Séaghdha, I. Leviant, R. Reichart, M. Gašić, A. Korhonen, and S. Young. Semantic specialization of distributional word vector spaces using monolingual and cross-lingual constraints. *arXiv preprint arXiv:1706.00374 Transactions of the Association for Computational Linguistics (TACL)*, 5:309–324, 2017 2017.
- [27] M. Nickel and D. Kiela. Poincaré embeddings for learning hierarchical representations. In *Advances in Neural Information Processing Systems (NeurIPS)*, 2017.
- [28] Z. Peng, Z. Li, J. Zhang, Y. Li, G. J. Qi, and J. Tang. Few-shot image recognition with knowledge transfer. In *International Conference on Computer Vision (ICCV)*, pages 441–449, 2019.
- [29] J. Pennington, R. Socher, and C. D. Manning. GloVe: Global vectors for word representation. In *Empirical Methods in Natural Language Processing (EMNLP)*, pages 1532–1543, 2014.
- [30] A. Radford, K. Narasimhan, T. Salimans, and I. Sutskever. Improving language understanding by generative pre-training. Technical report, OpenAI, 2018.
- [31] A. S. Razavian, H. Azizpour, J. Sullivan, and S. Carlsson. Cnn features off-the-shelf: An astounding baseline for recognition. *2014 IEEE Conference on Computer Vision and Pattern Recognition Workshops*, pages 512–519, 2014.
- [32] S. Rothe and H. Schütze. Autoextend: Combining word embeddings with semantic resources. *Computational Linguistics*, 43, 2017.
- [33] C. Szegedy, V. Vanhoucke, S. Ioffe, J. Shlens, and Z. Wojna. Rethinking the Inception architecture for computer vision. In *Computer Vision and Pattern Recognition (CVPR)*, pages 2818–2826, 2016.
- [34] C. Szegedy, S. Ioffe, V. Vanhoucke, and A. Alemi. Inception-v4, inception-resnet and the impact of residual connections on learning. *ArXiv*, abs/1602.07261, 2017.
- [35] P. Turaga and R. Chellapa. Nearest-Neighbor Search Algorithms on Non-Euclidean. *ICVGIP*, 2010.
- [36] X. Wang, Y. Ye, and A. Gupta. Zero-shot recognition via semantic embeddings and knowledge graphs. *arXiv preprint arXiv:1803.08035*, pages 6857–6866, 2018 2018.

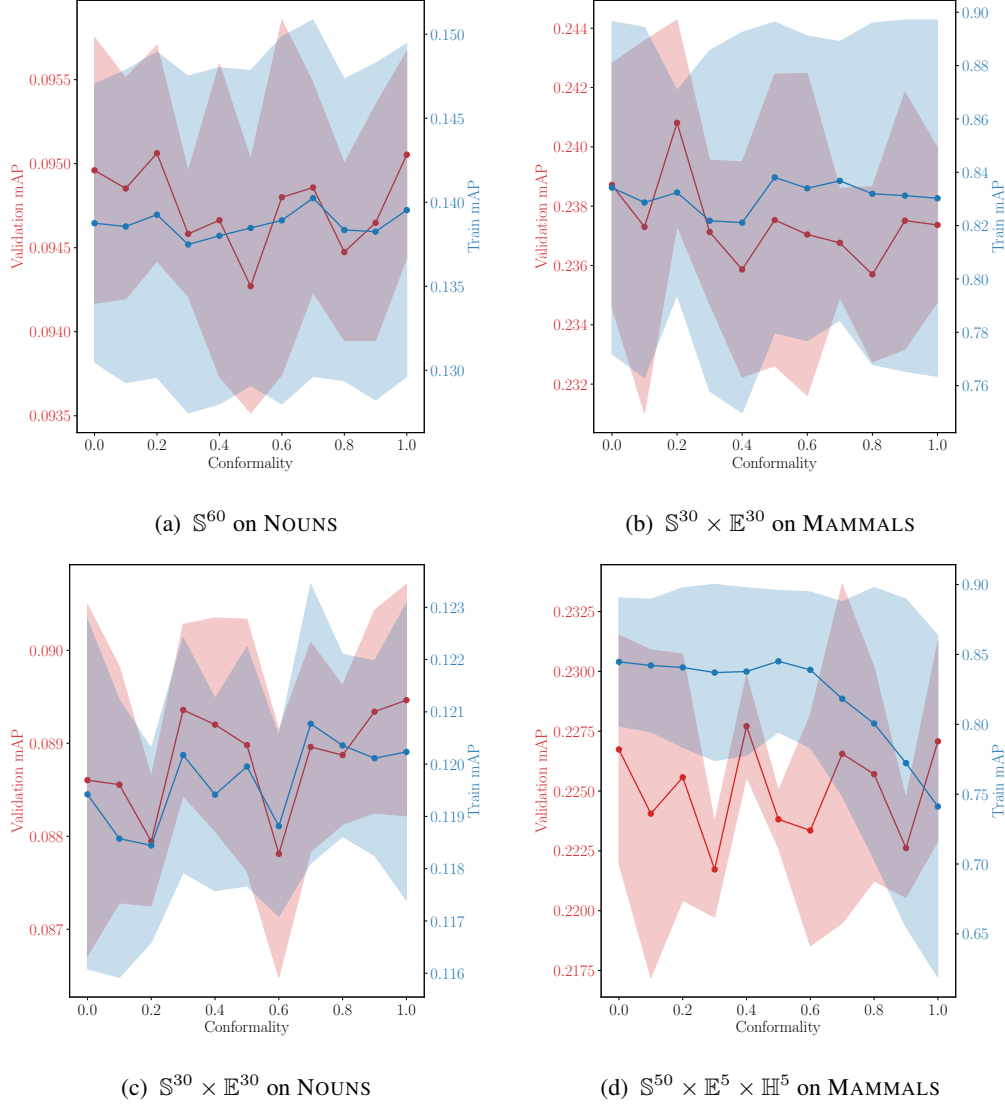


Figure 5: *Impact of conformality on train and validation mAP scores for top-performing target manifolds.* Each point is the average over 5 runs; the shaded region highlights a single standard deviation. We report conformality as  $-\log(C)$ , with a value of 0 corresponding to  $C = \infty$ , to better represent its range. Overall, we find that conformality plays a larger role for mixed manifolds, particularly for those containing a hyperbolic component.

## A Supplementary material: Conformal retrofitting via Riemannian manifolds

### A.1 Additional Dataset Statistics

Below are the additional dataset statistics for NOUNS and MAMMALS referenced in the main paper.

	Nodes	Edges	Mean Degree
Mammals	944 / 118 / 118	762 / 234 / 184	1.6 / 2.1 / 1.6
Nouns	65639 / 8211 / 8211	53572 / 14700 / 16155	1.6 / 1.9 / 2.1

## A.2 Hyperparameter Details

To discover the best hyperparameters for our models we performed random searches over several of them. We explored models with one to four Euclidean intermediate layers and layer sizes ranging from 100 to 1600. In a first pass, we found a layer size of 1600 and 3 hidden layers to work best; we fixed these parameters for subsequent experiments. We searched over several different target manifolds:  $\mathbb{S}^{60}, \mathbb{H}^{60}, \mathbb{E}^{60}, \mathbb{S}^{50}, \mathbb{H}^{50}, \mathbb{E}^{50}, \mathbb{S}^{45} \times \mathbb{H}^5, \mathbb{S}^{40} \times \mathbb{H}^5 \times \mathbb{E}^5, \mathbb{S}^{45} \times \mathbb{E}^5, \mathbb{S}^{50} \times \mathbb{E}^{10}, \mathbb{S}^{50} \times \mathbb{H}^{10}, \mathbb{S}^{50} \times \mathbb{H}^5 \times \mathbb{E}^5, \mathbb{S}^{30} \times \mathbb{H}^{30}, \mathbb{S}^{30} \times \mathbb{E}^{30}$ . We searched learning rates as well as GradNorm [4] weighting parameters within a linear scale. We searched conformality parameter values in the set:  $\{0.0, 0.2, 0.4, 0.6, 0.8, 1.0\}$ .

We have implemented all algorithms presented in the paper using PyTorch; the code will be made available with scripts to reproduce the results presented here upon acceptance. Our experiments were run on Amazon AWS instances and were orchestrated using Spell. Each instance had a single NVidia T4 GPU and 16GB of RAM. Experiments on the MAMMALS dataset were run for 2,000 epochs and took on average about 16 minutes. Experiments on the NOUNS dataset were run for 1,000 epochs (corresponding to 10,000 steps) and took on average about 5 hours and 45 minutes. We ran a net total of about 1,000 runs for the results presented in the paper.

## A.3 Proof of Theorem 1

Recall the constrained and unconstrained loss objectives for conformality defined in Section 3 of the main paper:

$$\begin{aligned}\ell_{\text{conf}}^{\text{constr.}}(p) &= \left\| \log \left( F_p G_p^{\mathcal{S}^{-1}} e^{-\alpha} \right) \right\|^2 \quad \text{subj. to } -C \leq \alpha \leq C, \\ \ell_{\text{conf}}^{\text{unconstr.}}(p) &= \left\| \log \left( F_p G_p^{\mathcal{S}^{-1}} \right) \right\|^2 - \begin{cases} \frac{1}{n} \log \det \left( F_p G_p^{\mathcal{S}^{-1}} \right)^2 & \text{if } \left| \frac{1}{n} \log \det \left( F_p G_p^{\mathcal{S}^{-1}} \right) \right| \leq C \\ 2C \left| \log \det \left( F_p G_p^{\mathcal{S}^{-1}} \right) \right| & \text{otherwise} \end{cases}.\end{aligned}$$

Here  $F_p$  denotes the pullback metric tensor,  $G_p^{\mathcal{S}}$  denotes the source metric tensor,  $C$  is the absolute upper bound on the relative difference between these two metric tensors, and  $\alpha$  is an additional optimization variable present in the constraints objective.

In the following lemma, we show optimize out  $\alpha$  to derive the unconstrained objective.

**Lemma 1.** *For any objective function  $J(\theta, \alpha) = \ell(\theta) + \ell_{\text{conf}}^{\text{constr.}}(p)$ ,  $\theta^*$  minimizes  $J(\theta, \alpha)$  iff it also minimizes  $J'(\theta) = \ell(\theta) + \ell_{\text{conf}}^{\text{unconstr.}}(p)$ .*

*Proof.* In general, we aim to optimize an objective of the form:

$$J(\theta, \alpha) = \ell(\theta) + \left\| \log \left( F_{\theta} G^{-1} e^{-\alpha} \right) \right\|^2,$$

where  $|\alpha| < C$ , and  $\ell(\theta)$  is some function which only depends on  $\theta$ ; for notational clarity, we have dropped  $p$  and  $\mathcal{S}$  and highlighted the  $\theta$  dependence of  $F$ .

We can simplify this objective as follows:

$$\begin{aligned}J(\theta, \alpha) &= \ell(\theta) + \left\| \log \left( F_{\theta} G^{-1} e^{-\alpha} \right) \right\|^2 \\ &= \ell(\theta) + \left\| \log \left( F_{\theta} G^{-1} \right) - \alpha I \right\|^2 \\ &= \ell(\theta) + \left\| \log \left( F_{\theta} G^{-1} \right) \right\|^2 - 2\alpha \text{tr} \{ \log \left( F_{\theta} G^{-1} \right) \} + \|\alpha I\|^2 \\ &= \ell(\theta) + \left\| \log \left( F_{\theta} G^{-1} \right) \right\|^2 - 2\alpha \log \det \left( F_{\theta} G^{-1} \right) + \alpha^2 n,\end{aligned}$$

where we have used Jacobi's formula:  $\text{tr} \log \left( F_{\theta} G^{-1} \right) = \log \det \left( F_{\theta} G^{-1} \right)$ .

For any  $\theta$ , and an unconstrained  $\alpha$ , we can solve for the optimal value of  $\alpha$ :

$$\begin{aligned}\frac{\partial J(\theta, \alpha^*)}{\partial \alpha} &= -2 \log \det \left( F_{\theta} G^{-1} \right) + 2\alpha^* n = 0 \\ \alpha^* &= \frac{1}{n} \log \det \left( F_{\theta} G^{-1} \right).\end{aligned}$$

Substituting in the original objective, we get:

$$\begin{aligned} J(\theta) &= \ell(\theta) + \left\| \log(F_\theta G^{-1}) \right\|^2 - 2 \frac{1}{n} \log \det(F_\theta G^{-1}) \log \det(F_\theta G^{-1}) + \frac{1}{n^2} \log \det(F_\theta G^{-1})^2 n \\ &= \ell(\theta) + \left\| \log(F_\theta G^{-1}) \right\|^2 - \frac{1}{n} \log \det(F_\theta G^{-1})^2. \end{aligned}$$

Note that  $J(\theta, \alpha)$  is quadratic in  $\alpha$ : when  $\frac{1}{n} |\log \det(F_\theta G^{-1})| > C$ , the optimal value of  $J(\theta, \alpha)$  will be at the boundary:  $\alpha^* = \text{sgn}(\log \det(F_\theta G^{-1})) C$ . As a result:

$$J(\theta) = \ell(\theta) + \left\| \log(F_\theta G^{-1}) \right\|^2 - 2C |\log \det(F_\theta G^{-1})| + C^2 n.$$

Combining these two cases, we get the final result:

$$J(\theta) = \ell(\theta) + \left\| \log(F_\theta G^{-1}) \right\|^2 - \begin{cases} \frac{1}{n} \log \det(F_\theta G^{-1})^2 & \text{if } \left| \frac{1}{n} \log \det(F_\theta G^{-1}) \right| \leq C \\ 2C |\log \det(F_\theta G^{-1})| & \text{otherwise} \end{cases}.$$

□

**Theorem 2.** For all values of  $C$ ,  $f$  is a conformal map iff  $\ell_{\text{conf}}(p) = 0$  for all points  $p \in \mathcal{S}$ ; if  $C = 0$ , then  $f$  is a isometric map iff  $\ell_{\text{conf}}(p) = 0$  for all points  $p \in \mathcal{S}$ .

*Proof.* Suppose  $C = 0$ . If  $\ell_{\text{conf}}(p) = 0$  for all points  $p$  then,

$$\left\| \log(F_p G_p^S) \right\|^2 = 0$$

for all points  $p$ . This is true if and only if the geodesic distance between  $F_p$  and  $G_p^S$  on the manifold of positive definite matrices equals zero which is true if and only if  $F_p = G_p^S$ . Having a pullback metric that is equal to the metric on the original space is the definition of an isometric map between Riemannian manifolds. This can be seen to align with the intuitive definition of an isometry—a function that preserves distances. For any two points  $p_1, p_2$  we see that the distances are preserved:

$$\begin{aligned} d^S(p_1, p_2) &= \min_{\gamma} \int_0^1 \sqrt{G_{\gamma(t)}^S(\dot{\gamma}(t), \dot{\gamma}(t))} dt \\ &= \min_{\gamma} \int_0^1 \sqrt{F_{\gamma(t)}(\dot{\gamma}(t), \dot{\gamma}(t))} dt \\ &= \min_{\gamma} \int_0^1 \sqrt{G_{f(\gamma(t))}^T(df(\dot{\gamma}(t)), df(\dot{\gamma}(t)))} dt = d^T(f(p_1), f(p_2)) \end{aligned}$$

where  $G^T$  is the target manifold metric tensor and  $\gamma$  is any smooth curve connecting  $p_1, p_2$ . The Myers–Steenrod theorem gives the converse: that every distance preserving map between Riemannian manifolds is necessarily a smooth isometry of Riemannian manifolds and has a pullback metric equal to the metric on the original space.

Now, suppose  $C$  is any value. By similar logic, the loss is nonzero if and only if the geodesic distance between  $F_p$  and  $e^\alpha G_p^S$  is zero. This is true if and only if  $F_p = e^\alpha G_p^S$  which is the requirement by definition for a map between Riemannian manifolds to be considered conformal. We can see this aligns with the traditional definition of conformal: angles between tangent vectors are preserved as for any tangent vectors  $v_1, v_2$  at a point  $p$ :

$$\begin{aligned} \cos_G(\theta(v_1, v_2)) &= \frac{G_p^S(v_1, v_2)}{\sqrt{G_p^S(v_1, v_1) G_p^S(v_2, v_2)}} \\ &= \frac{e^\alpha G_p^S(v_1, v_2)}{\sqrt{e^\alpha G_p^S(v_1, v_1) e^\alpha G_p^S(v_2, v_2)}} \\ &= \frac{F_p(v_1, v_2)}{\sqrt{F_p(v_1, v_1) F_p(v_2, v_2)}} = \cos_F(\theta(v_1, v_2)), \end{aligned}$$

where  $\cos_G(\theta(v_1, v_2))$  and  $\cos_F(\theta(v_1, v_2))$  measure the cosine of the angles between  $v_1$  and  $v_2$  according to the source metric  $G_p^S$  and pullback metric  $F_p$ . In other words, any map which preserves angles between any tangent vectors at every point must have a pullback metric that is a positive scalar multiple of the source metric at every point.  $\square$